Kinetics of Singlet Oxygen Release from Endoperoxides of 2-Pyridone Derivatives

A Major Qualifying Project Report:

submitted to the Faculty

of the

WORCESTER POLYTECHNIC INSTITUTE

in partial fulfillment of the requirements for the

Degree of Bachelor of Science in Chemistry

By

Lan Luo

Date: May 3, 2011

Approved:

Professor Robert E. Connors, Advisor

Table of Contents

List of Figures

List of Tables

Abstract

Singlet oxygen can decompose toxic substances by oxidation, but its direct generation from atmospheric oxygen by a photosensitizer requires a light source. In this project, six derivatives of 2-pyridone that can reversibly trap singlet oxygen under irradiation and release it in the dark were studied. The rates of thermolysis of their endoperoxides were measured by UV-Vis spectroscopy. Theoretical modeling was also carried out with Gaussian 09. Overall, *N*-isoamyl-2-pyridone has the best release performance. This study also evaluates the effects of sterics and electronics on this trend, and discusses the possibility of theoretical modeling to evaluate *N*-substituted 2-pyridones. Pyridone samples investigated in this study were provided by Ventana Research Corporation.

Acknowledgements

I would like to thank Dr. Chuchawin Changtong for his advice on the kinetics study of singlet oxygen and the synthesis of pyridone derivatives, and Professor Robert E. Connors for his guidance and support throughout the project. I would also like to thank Professor James W. Pavlik, Professor James P. Dittami, Zhen Chen, and Christopher Zoto for their thoughtful advice.

Introduction

Singlet oxygen has been studied extensively over the years by scientists for its oxidizing properties. By reacting with toxic chemical agents such as the mustard gas, they can form less toxic or harmless substances. This has large applications in protection against chemical and biological attacks. In addition, incorporating singlet oxygen generating compounds into fabrics has demonstrated great self-detoxification. Together with superhydrophobic surfaces, these self-cleaning novel materials have great promise in the future. In the past, singlet oxygen has been applied in chemical lasers as an energy source and in photodynamic therapy, which has been proven to treat cancer in esophagus and the early stages of bronchus.[i]

However, since the production of singlet oxygen requires the continued presence of light, photosensitizer and oxygen, controlling the generation of singlet oxygen under other conditions is thus of particular interest. Compounds such as 2-pyridone and naphthalene can react with singlet oxygen via [4+2] cycloaddition to form the endoperoxide adducts, which would decompose to form the original compound and singlet oxygen upon heating. This provides a way to generate singlet oxygen at times when a light source is absent.

Previous works in this field include those of Wasserman [1], Aubry [2], and Chuchawin [3]. While Wasserman [1] concluded electron density as a determinant for endoperoxide formation and sterics as an important factor for its stability, Aubry [2] found electron donating groups on polycyclic compounds favorable for endoperoxide formation. Chuchawin [3], on the other hand, synthesized a large group of 2-pyridone derivatives and measured the thermolysis of their endoperoxides at 40 ℃.

This project focused on two specific groups of the N-substituted 2-pyridones, with an isoamyl group or a 2-methoxy-2-oxoethyl group attached to the nitrogen. By employing the Arrhenius and Eyring equations, rate constants at different temperatures can be extrapolated without the need of more

[i] http://www.photobiology.com/educational/len2/singox.html

thermolysis experiments. Moreover, as an effort to reduce human labor, predicting power of the Gaussian program in calculating the kinetics parameters were also tested at B3LYP/6-311+G* level of theory.

Background

Singlet Oxygen

Molecular oxygen is one of the most abundant substances on the earth, occupying more than 20% of the air. The molecular orbital (Figure 1) of this stable oxygen in triplet state, demonstrates its paramagnetism, where the HOMO of the atom has two unpaired electrons. Singlet oxygen, on the other hand, shows diamagnetism.

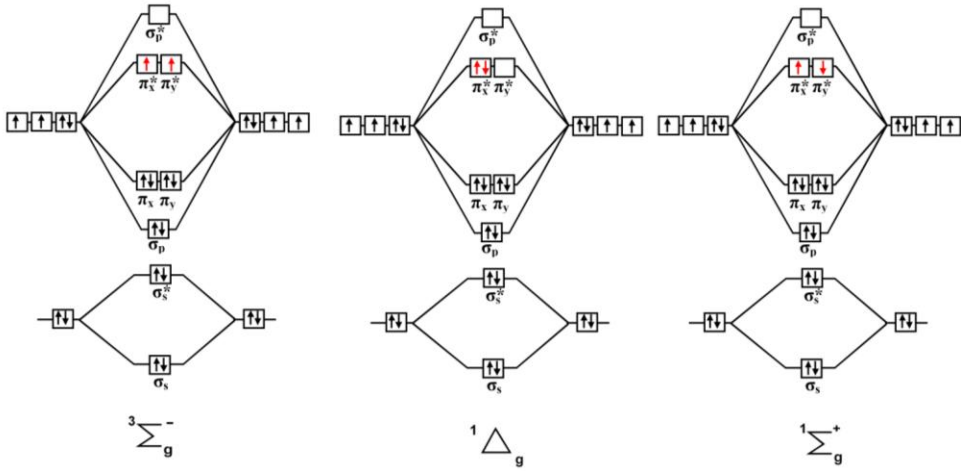

Figure 1: Molecular orbital of triplet ground state oxygen ($^3\sum_g^-$), higher energy singlet oxygen ($^1\sum_g^+$), and lower energy singlet oxygen ($^1\Delta_g$) from left to right. [ii]

By giving these triplet state oxygen ($^3\sum_g^-$) an excitation energy of 22.5 kcal/mole,[iii] these molecules can be excited to the higher energy singlet state ($^1\sum_g^+$), which is then rapidly converted to lower energy singlet oxygen ($^1\Delta_g$). The conversion of singlet oxygen back to triplet oxygen, on the opposite process, shows metastability, where it requires an input of energy to induce a transition ($^1\sum_g^+$) from the existing metastable state ($^1\Delta_g$) before converting to the most stable state ($^3\sum_g^-$).

Since the conversion from the triplet oxygen to the singlet state requires a spin flip which is forbidden (low probability), or vice versa, both triplet and singlet state oxygen have relatively long

[ii] http://en.wikipedia.org/wiki/Singlet_oxygen
[iii] http://www.photobiology.com/educational/len2/singox.html

lifetimes. Singlet oxygen is thus more commonly generated via chemical processes or the use of a photosensitizer.

By reacting hydrogen peroxide with hypochloride, part of the free energy from the reaction is put into the excitation of oxygen molecules, which is known as chemiluminescence. Singlet oxygen can be also generated by the decomposition of hydrogen trioxide in water[iv], phosphite ozonides and endoperoxides[v].

In the experiments described here, singlet oxygen is produced via energy transfer from tetraphenylporphyrin (Fig 3), which is a photosensitizer. Resembling chlorophyll, the porphyrin molecule absorbs light and is promoted into the excited singlet state. And through intersystem crossing, the excited singlet sensitizer can spin-flip to a lower energy triplet state. This process will result in an energy transfer from the porphyrin triplet state to the triplet state oxygen, promoting it to the excited singlet state.

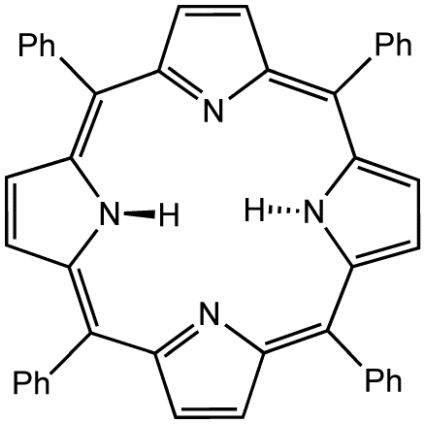

Figure 2: Structure of Tetraphenylporphyrin.

Pyridones

[iv] http://en.wikipedia.org/wiki/Singlet_oxygen
[v] http://www.photobiology.com/educational/len2/singox.html

Pyridones are organic compounds that have an amide as well as a keto group. 2-Pyridone, which has the keto group located on the second position, can undergo tautomerism to form 2-hydroxypyridine, which is readily available from commercial companies.

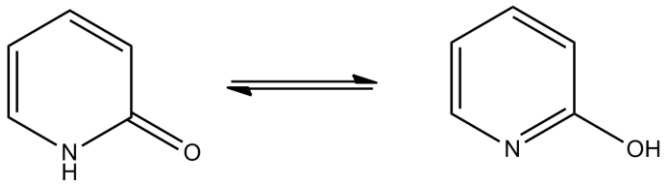

Figure 3: Tautomerism of 2-pyridone.

By deprotonating the 2-pyridone with a base, this compound can easily perform nucleophilic attack to form a series of N-substituted 2-pyridones.

These N-substituted 2-pyridones can undergo [4+2] cycloaddition, which resembles the Diels-Alder reaction, to form endoperoxide adducts. The trapping efficiency of singlet oxygen can vary by 10 fold in compounds with different electronic density. Upon heating, the endoperoxides decompose to form the corresponding pyridones and singlet oxygen in high yield.

Experimental

Kinetic parameters by UV-Vis spectroscopy

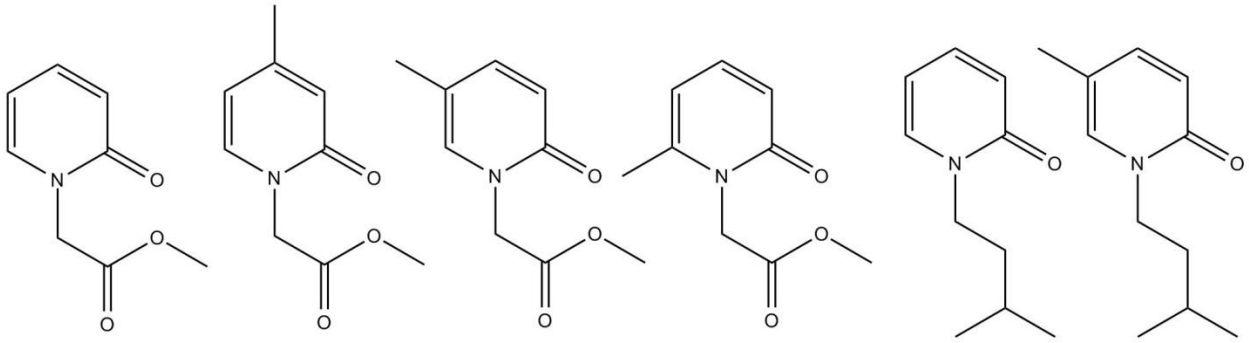

Figure 4: Structures of investigated pyridones: 1a, 1c, 1d, 1e, 2a, 2d (from left to right).

Experimental procedures

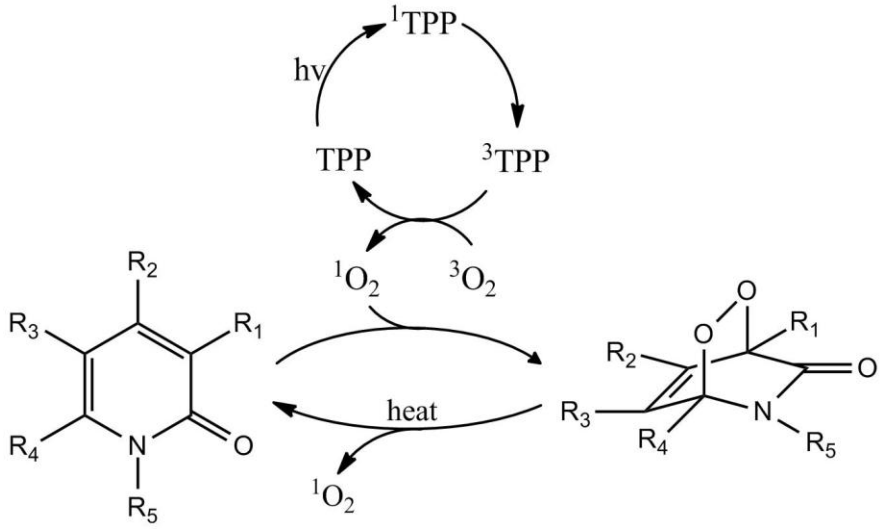

Figure 5: Illustration of the experiment.

Pyridones absorbs at a wavelength of about 303nm in chloroform. Since the endoperoxide does not absorb at the same region as pyridone, the peak at 303nm can be used to monitor the concentration of pyridone over time. The concentration of the endoperoxide can be then easily converted to that of the pyridone, leading to the kinetics of the thermolysis.[3] The detailed conversions and calculations are in the Reaction Rate section.

In the experiment, a solution of the pyridone sample was prepared in chloroform at a concentration that absorbs at between 0.8 and 1.2 absorbance units (as 2a in Figure 6). A catalytic amount of tetraphenylporphrin (TPP) was added to the cuvette and recorded in the UV-Vis spectroscopy (as 2a+TPP in Figure 6) before the irradiation.

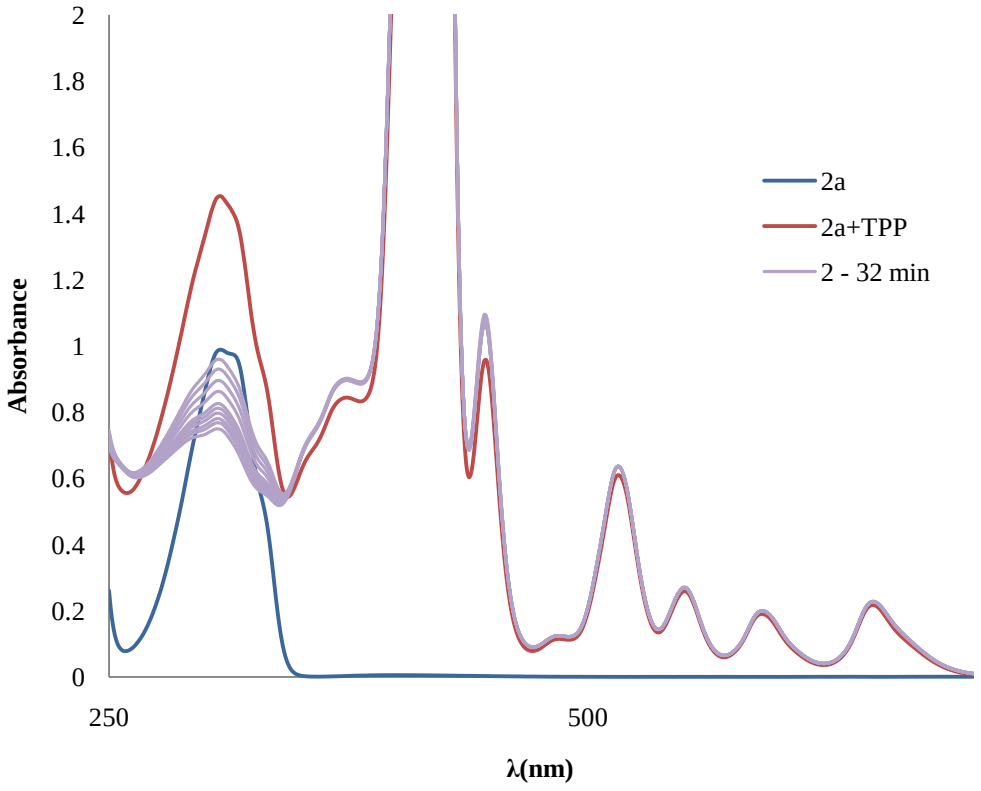

Figure 6: UV-Vis spectra of pyridone 2a (blue), 2a+TPP (red) and the 2a+TPP during the thermolysis at 40.1 ℃ (purple).

When the solution was irradiated under a Xenon arc lamp with a filter ($\lambda > 500$ nm), oxygen was bubbled simultaneously into the cuvette, in which the endoperoxide adduct was formed. The cuvette was then placed in a temperature-controlled UV-Vis spectrophotometer, where the endoperoxide adduct was allowed to decompose isothermally. UV-Vis spectra (Figure 7) of the sample were taken at regular intervals to monitor the thermolysis. As the endoperoxide reverts back to the pyridone, a gradual increase in the absorbance at 303nm was observed.

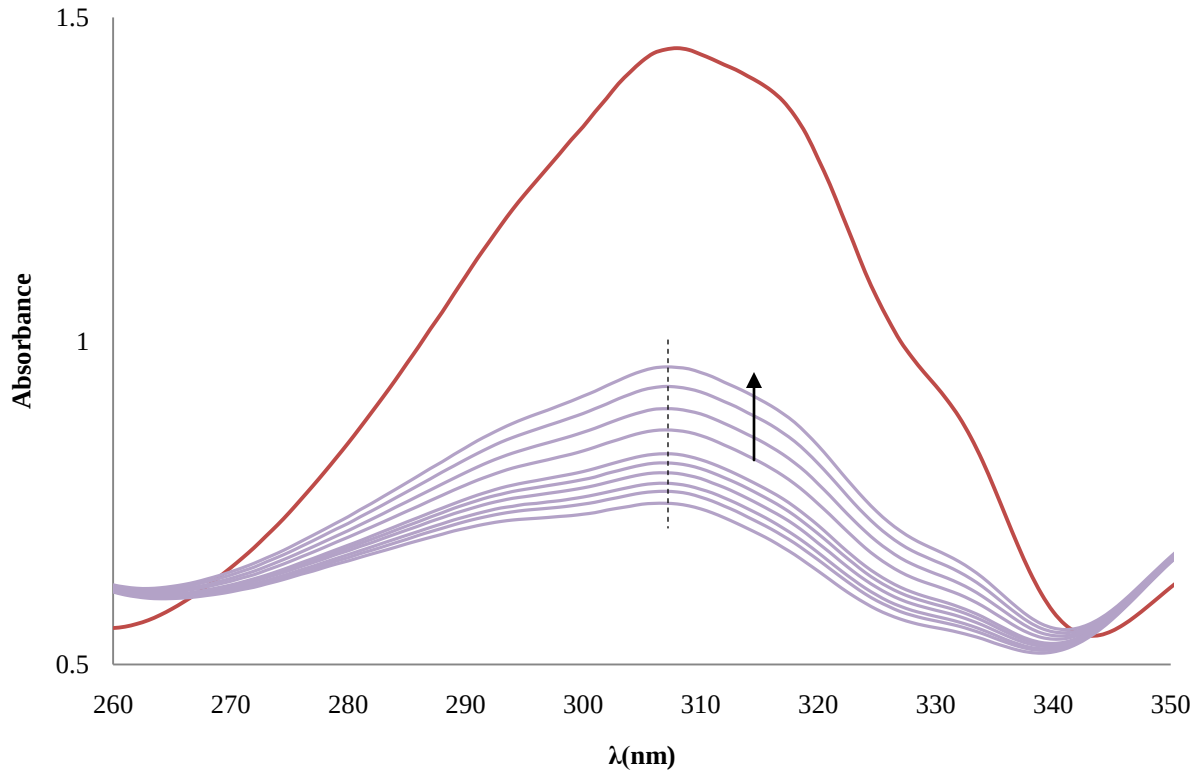

Figure 7: UV-Vis spectra of the increase in pyridone concentration during the thermolysis of endoperoxide 2a at 40.1 ℃.

Reaction Rate

We will start by defining a few terms:

$[Pyridone]_{total}$ = concentration of pyridone before the irradiation

$[Pyridone]_0$ = concentration of pyridone at time zero of the thermolysis

$[Pyridone]_t$ = concentration of pyridone at time t of the thermolysis

$[Endo]_0$ = concentration of endoperoxide at time zero of the thermolysis

$[Endo]_t$ = concentration of endoperoxide at time t of the thermolysis

[TPP] = concentration of TPP

A_{before} , A_{after} = Absorbance of peak at around 303nm before and after the irradiation

ΔA_0, ΔA_t = difference between A_{before} and A_{after} at time 0 and t

ε_{TPP}, $\varepsilon_{pyridone}$ = extinction coefficient of TPP and pyridone

l = cell length

The thermolysis of the endoperoxide adducts follows a first order reaction kinetics. Thus, the integrated first-order rate law is

$$\ln[Endo]_t = - kt + \ln[Endo]_0 \text{ ----------1}$$

However, the concentration of the endoperoxide cannot be directly measured by the UV-Vis spectrophotometer, since it does not absorb light significantly. Thus it was indirectly obtained from the concentration of pyridone, which absorbs at around 300nm.

$$[Endo]_t = [Endo]_0 + [Pyridone]_0 - [Pyridone]_t \text{----------2}$$

Since TPP and pyridone absorbs at the same region at around 300nm, the absorbance at 300nm in the spectra equals the absorbances from both TPP and pyridone at this wavelength. [4]

$$A_{mixture} = \varepsilon_1 \times l \times C_1 + \varepsilon_2 \times l \times C_2$$

Given the above information, a spectrum was taken before irradiation under the Xenon lamp, where

$$A_{before} = \varepsilon_{TPP} \times l \times [TPP] + \varepsilon_{pyridone} \times l \times [Pyridone]_{total} \text{----------3}$$

After irradiation to give maximum consumption of the pyridone to form the adduct,

$$[Pyridone]_{total} = [Endo]_0 + [Pyridone]_0 \text{ ----------4}$$

A sequence of spectra was then taken at some time interval to construct the decay rate, where

$$A_{after} = \varepsilon_{TPP} \times l \times [TPP] + \varepsilon_{pyridone} \times l \times [Pyridone]_t \text{----------5}$$

From equation 2 & 4,

$$[Pyridone]_{total} - [Pyridone]_t = [Endo]_0 + [Pyridone]_0 - [Pyridone]_t = [Endo]_t \text{ ----------6}$$

Subtracting equation 5 from 3, and referring to 6,

$$\Delta A_t = A_{before} - A_{after} = \varepsilon_{pyridone} \times l \times [Endo]_t \text{----------7}$$

Taking the logarithm of both sides of the equation 7,

$$\ln [\Delta A]_t = \ln [Endo]_t + C = -kt + \ln [Endo]_0 + C$$

Therefore, ploting $\ln [\Delta A]_t$ against time would give the rate constant k as the negative of the slope. The detailed results of the thermolysis experiment are found in Appendix A.

Arrhenius Plots

The Arrhenius equation, which expresses the temperature dependence of the reaction rate constant, was employed to calculate the activation energy of the conversion of the endoperoxide adduct to the pyridone.

$$\ln(k) = \frac{-E_a}{R}\frac{1}{T} + \ln(A)$$

The results can be found in Appendix B.

Eyring Plots

The Eyring equation was utilized to show enthalpy and entropy differences between the endoperoxide adduct and the transition state of the conversion. The differences can be calculated from the slope and y-intercept.

$$ln\frac{k}{T} = \frac{-\Delta H^{\ddagger}}{R}\frac{1}{T} + ln\frac{k_B}{h} + \frac{\Delta S^{\ddagger}}{R}$$

The detailed plots can be found in Appendix B.

Molecular Modeling (Gaussian 09 Software Package)

Theoretical calculations were performed by Gaussian 09, a program commercially available that predicts energies, molecular structures, vibrational frequencies, and many more molecular properties. It is based on the fundamentals of quantum mechanics and is employed by others [1] in the field. Density functional theory (DFT) calculations were performed at the B3LYP/6-311+G* level of the theory.

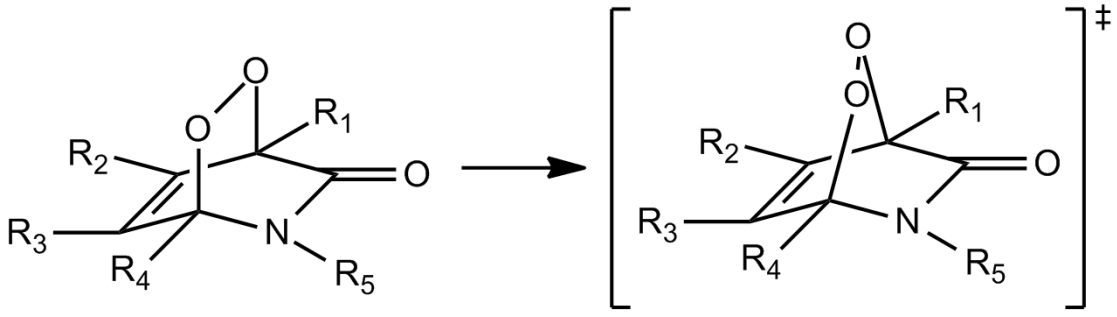

Figure 8: Activation step for the thermolysis of the endoperoxide adducts.

Geometric optimization was performed for the endoperoxide adduct in chloroform, after which the vibration frequencies were calculated. Either the transition state optimization or the saddle point calculation was used to find the optimized structure of the transition state, which is a

local maximum. To verify that it has reached a local maximum, vibrational frequencies for this transition state were calculated, ensuring the existence of only one negative vibrational frequency which corresponds to the stretching of two C-O bonds. (Transition state test)

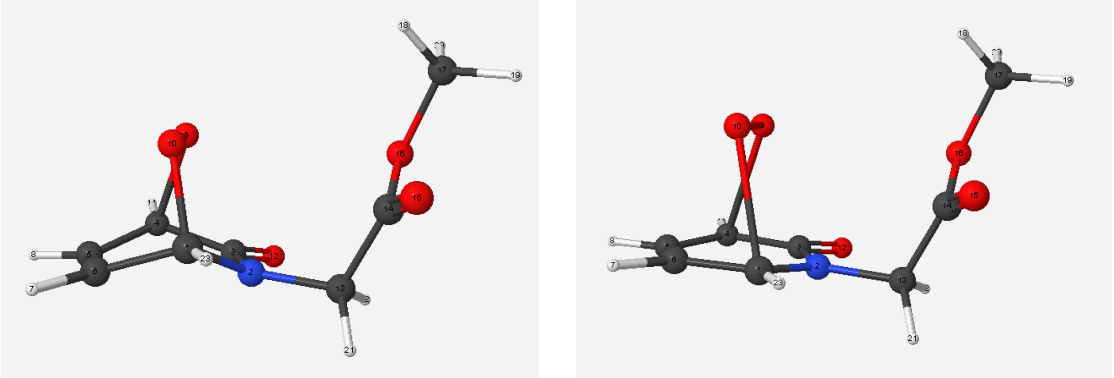

Figure 9: An illustration of the negative vibrational mode in the Transition State Test of compound 1a.

The activation energy for the reaction was obtained by taking

$$E_a = E_{\text{transition state}} - E_{\text{endoperoxide}}$$

Similar operations were also performed to retrieve theoretical $\Delta H^{\ddagger}$, $\Delta G^{\ddagger}$, $\Delta S^{\ddagger}$.

Synthesis of N-substituted Pyridones

1-(Hydroxymethyl)-2(1H)-pyridinone

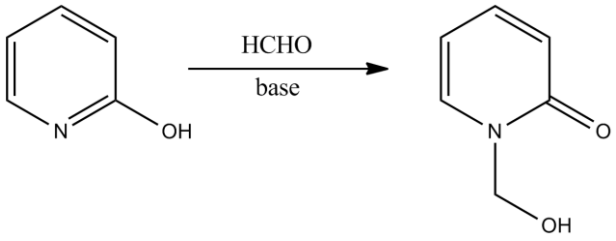

A stock solution of KOH (pH=14) was made by dissolving KOH in an appropriate amount of water. A portion of the solution was then adjusted to pH=9 by dilution. In a round

bottom flask (50ml) 2-hydroxypyridine (0.951g) was dissolved in the KOH solution (pH=9, 20ml) and stirred under room temperature. The pH was measured again and adjusted to 9 using the stock KOH solution. Formalin (1ml) was added dropwise into the flask over a period of 30 minutes using a dropping funnel. This dropwise addition of the formalin minimizes consumption of formalin by base to form formic acid and methanol. The reaction was stirred vigorously in the closed flask for 24 hours. During the process, three more portions of formalin (1ml each) were slowly added to the reaction in the same manner. Monitoring of the experiment is not viable by TLC, because the starting material and product have very similar R_f values in many solvents, ranging from non-polar to polar ones.

The resulting solution was adjusted to pH=6 by adding HCl (25% HCl) and was extracted by dichloromethane using a separatory funnel. In this process, dichloromethane (10 ml each, twice) was used and stored in an Erlenmeyer flask (250ml). Since the product is highly soluble in water, to get most of the product out, the water layer was saturated with NaCl and rotavaped to dryness. NaCl will break the hydrogen bond between the desired product and water so that it would not escape with the water during the evaporation. The dried residue was then washed with dichloromethane (10ml, twice) and ethyl acetate (10ml, once). The mixture was combined with the previous dichloromethane in the Erlenmeyer flask and rotavaped to dryness. The crude product was then recrystalized in dichloromethane.

1-(Hydroxymethyl)-5-methyl-2(1H)-pyridinone

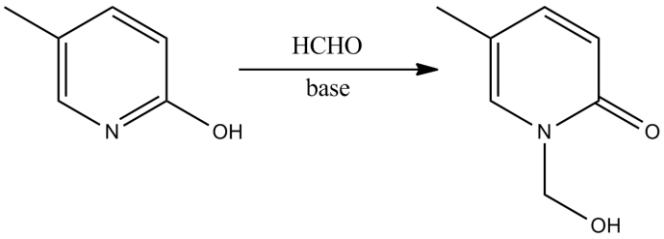

KOH (0.0116mol, 0.65g) was added into a solution (approximately 20ml) of 5-methyl-2(1H)-pyridinone (5mmol, 0.55g) and stirred in round bottom flask (100ml). The solution turned pale yellow after the addition of base. Formalin (37%, 10ml) was then added dropwise into the stirring flask over a period of 15 minutes. The reaction flask was sealed and allowed to run for 24 hours to avoid absorption of CO_2.

The resulting solution was adjusted to pH=6, in which the solution turned clear, and was then extracted with dichloromethane (three times, 15ml each) in a separatory funnel. The aqueous layer was saturated with NaCl and extracted again with dichloromethane (three times, 15ml each). The process was continued until the aqueous layer can no longer dissolve NaCl. The dichloromethane solution was then rotavaped to dryness and recrystalized in dichloromethane to give a white solid. Yield = 0.3033g, impurity about 15%.

Results and Discussions

Experimental and Theoretical Results

To allow further conclusions on the efficiency of these pyridones in trapping and releasing singlet oxygen, we first have to examine the reliability of the results by comparison among the various sources. The reaction rate constant at 40.0 ℃ from Gaussian 09, experiments and other source[3] are presented. (Table 1)

Endoperoxide	**Rate constant at 40.0 ℃ (10^{-5} s^{-1})**		
	Gaussian 09	Experimental	Chuchawin[3]
1a	2	4.1	4
1c	65	2.6	2
1d	39	1.5	2
1e	170	4.1	3
2a	20	21.0	20
2d	3100	12.0	10

Table 1: Reaction rate constants of the thermolysis from Gaussian 09, experiments and other source[3].

The reliability of experimental results is high since the rate constant agrees well with the data provided by Ventana Research Corporation. However, the quality of theoretical results varies. There are some inconsistencies between Gaussian and the experimental results; the largest difference is in compound 2d where the rate constant in Gaussian is about 258 times as much as that of the experiment. Despite the large discrepancies, some agreements were shown in compounds that do not have a methyl substituent on the carbon positions of the ring: compound 1a and 2a.

The disagreement between theoretical and experimental results might be attributable to the limitations of Gaussian as an effective tool to reproduce the energy of the singlet oxygen

generated in the thermolysis.[1] However, this cannot explain the fact that there is indeed some agreement in compound 1a and 2a.

Thermodynamic activation parameters are also tabulated below for comparison. And the free energy changes are quantities of interest because they are directly related to the reaction rate constant *k* at any specific temperature via the Eyring equation.

Endoperoxide	**Activation parameters (Experimental)**			
	E_a kcal/mol	$\Delta H^{\ddagger}$ kcal/mol	$\Delta G^{\ddagger}$ kcal/mol	$\Delta S^{\ddagger}$ cal/mol ⁄K
1a	23.1	22.5	24.5	-6.9
1c	22.9	22.3	24.8	-8.4
1d	29.7	29.1	25.5	12.2
1e	25.4	24.8	24.7	0.4
2a	25.9	25.3	23.7	5.3
2d	27.0	26.3	24.1	7.5

Table 2: Experimental thermodynamic activation parameters.

Endoperoxide	**Activation parameters (Gaussian 09)**			
	E_a kcal/mol	$\Delta H^{\ddagger}$ kcal/mol	$\Delta G^{\ddagger}$ kcal/mol	$\Delta S^{\ddagger}$ cal/mol ⁄K
1a	26.8	25.9	25.1	2.7
1c	25.4	23.8	22.9	3.1
1d	24.6	23.0	23.3	-0.9
1e	23.6	22.4	22.3	0.3
2a	24.7	23.7	23.5	0.5
2d	22.7	21.1	20.5	1.9

Table 3: Theoretical (Gaussian 09) thermodynamic activation parameters.

In sum, experimental data and external source (Table 4) show that pyridone 2d is the fastest in trapping singlet oxygen, while pyridone 2a is the fastest in releasing singlet oxygen. Overall, compound 2d is the best performing pyridone.

	k at 40.0 ℃ (10^{-5} s^{-1}) (Experiment)	Trap rate[3]
1a	4.1	-91% in 65 min
1c	2.6	-100% in 120 min
1d	1.5	-100% in 8 min
1e	4.1	-97% in 10 min
2a	21.0	-100% in 60 min
2d	12.0	-100% in 6 min

Table 4: Trapping and releasing efficiencies of various endoperoxide adducts.

Release of Singlet Oxygen

Of the six compounds studied in this project, endoperoxides with an isoamyl group (2a and 2d) on the nitrogen decompose faster than those with a 2-methoxy-2-oxoethyl group (1a, 1c, 1d and 1e). (Table 4) In order to rationalize the observed experiment results, a theoretical study was performed in Gaussian 09 to investigate the effects of electron density and steric factors in the stability of the endoperoxides. Pyridones without substituents on the carbon positions on the ring were selected because of the relative higher accuracy of data.

Endoperoxide	**Substituent effect (Gaussian 09)**				
	E_a kcal/mol	$\Delta H^{\ddagger}$ kcal/mol	$\Delta G^{\ddagger}$ kcal/mol	$\Delta S^{\ddagger}$ cal/mol K	*k* (40 ℃) ($10^{-5}s^{-1}$)
$-CH_2OH$ (1)	20.49	19.15	19.17	-0.08	2.7×10^{-1}
$-CH_3$ (2)	21.75	20.27	19.90	1.24	8.4×10^{-2}
$-CH_2Cl$ (3)	24.58	22.98	22.36	2.08	1.6×10^{-3}

Table 5: Summary of theoretical calculations of the thermodynamic activation parameters and reaction rate constants of the substituent effect study.

From the theoretical calculations, the endoperoxide of *N*-hydromethyl-2-pyridone (pyridone 1) has the fastest release of singlet oxygen, followed by those of *N*-methyl-2-pyridone (pyridone 2) and *N*-chloromethyl-2-pyridone (pyridone 3).

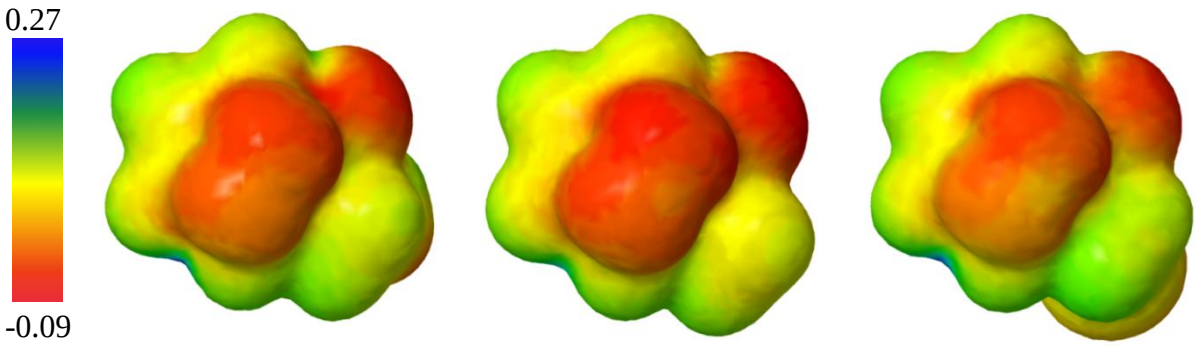

Figure 10: The electrostatic plots of the transition states of the endoperoxide of *N*-hydromethyl-2-pyridone, *N*-methyl-2-pyridone and *N*-chloromethyl-2-pyridone (from left to right).

Looking at the electrostatic plots of the transition states of the thermolysis of these endoperoxides (Figure 10), the structure in the middle, which corresponds to the endoperoxide of pyridone 2, has the largest electron density on the two peroxide oxygen, thus should demonstrate the biggest potential in release. However, the calculated trend (Table 5) cannot be explained by these plots (Figure 10).

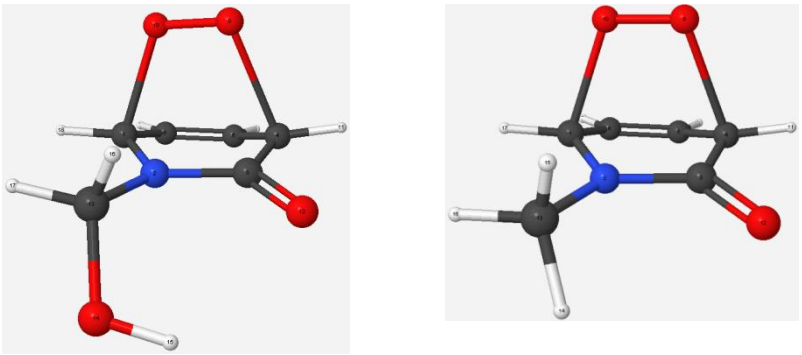

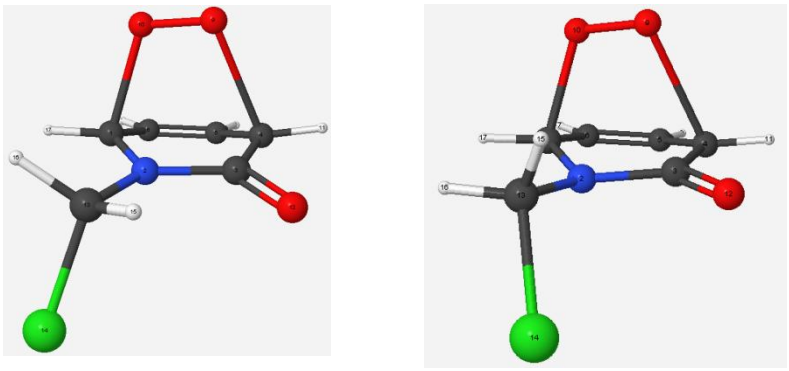

Figure 11: Structures of the transition states of the endoperoxides of *N*-hydromethyl-2-pyridone (top left) , *N*-methyl-2-pyridone (top right), *N*-chloromethyl-2-pyridone (top left) and a modified *N*-chloromethyl-2-pyridone (top right).

By comparing the structures of the transition state, the hydroxymethyl group of pyridone 1 has the largest interference with the molecule compared with the other two pyridones, whose substituents point away from the ring. What is more interesting is turning the chloromethyl group towards the molecule (bottom right of Figure 11) and subsequently perform the transition state optimization, the bond lengths of the two peroxide oxygen and the attached carbons, increased from 1.915Å and 2.220Å to 1.920Å and 2.354Å, suggesting a higher release rate of singlet oxygen.

These preliminary results imply steric factor as important in the release of singlet oxygen and that its effect might be larger than the electronic factor. However, future work needs to be done to determine the relative importance of steric and electronic influences.

Trapping of Singlet Oxygen

Aubry *et al.*[2] suggest that electron donating groups substituted on polycyclic aromatic compounds promote endoperoxide formation, thus increasing the trapping efficiencies of these materials. Since singlet oxygen is a highly electrophilic species, the formation of endoperoxide

thus can be related to the electronic nature of the substrate.[1] From qualitative data obtained from Ventana Research Corporation (Table 4) the methyl (electron donating) substituted pyridone 1d, 1e and 2d demonstrate efficiency in trapping singlet oxygen, with the majority converted to the endoperoxides in less than 10 minutes. That is, methyl group substitution at positions 5 and 6 enhance the trapping efficiency of the pyridone by six to eight times. However, compound 1c, which has a methyl group substituted on position 4, is far less capable of trapping singlet oxygen. The experimental trapping results obtained by Ventana suggest that the electronic effect described by Aubry depend on the ring position where the methyl group is bonded.

Conclusion

Experimental data shows pyridone 2d and 2a are the best at trapping and releasing singlet oxygen, respectively. In general, a methyl group substituted on the pyridone ring at position 5 and 6 tends to promote the trapping of singlet oxygen, while a methyl group at position 4 reduces the trapping efficiency. And pyridones with an isoamyl group on the nitrogen tends to result in a less stable endoperoxide with faster release of singlet oxygen than one with a 2-methoxy-2-oxoethyl group.

Theoretical modeling (Gaussian 09) is more accurate in predicting kinetic parameters for 2-pyridones that do not have a methyl substituent on the carbon positions of the ring.

Although the exact nature of substituent effect is uncertain, preliminary results suggest that steric factor is a contribution and that it may have greater influence than the electronic effect.

Future Work

On the synthesis of more pyridones, bulkier groups (such as phenyl and naphthalene) closer to the nitrogen can be substituted on the ring to investigate steric factor in the release of singlet oxygen. A study using unbranched and branched alkyl groups can also be conducted to test the influence of sterics. On the other hand, an electron donating or electron withdrawing group can be attached at the various carbon positions of the ring to examine the electronic effect. Some of the potential targets include these molecules listed below.

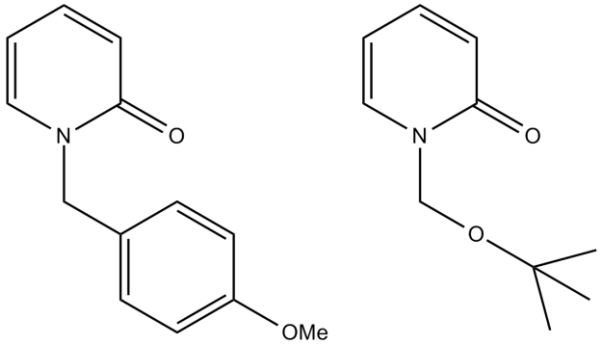

Figure 12: Potential synthetic targets.

For the kinetic study on the thermolysis of the endoperoxides, different solvents can be used to compare the change in the rate of the decomposition.

The capability of Gaussian in calculating useful parameters can be explored further, including its ability to calculate bond length, bond order and atom distances.

Appendix A – First Order Kinetics Plots

Pyridone 1a

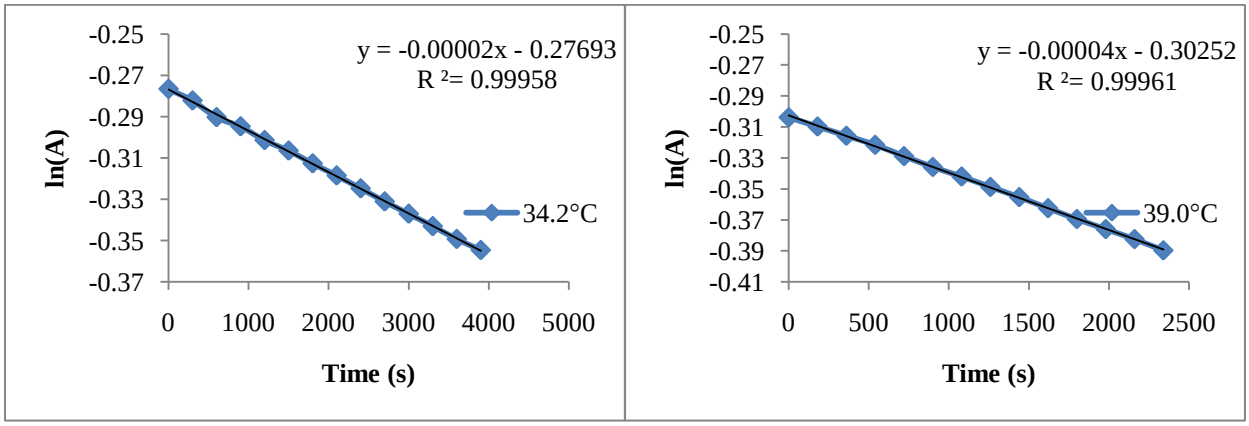

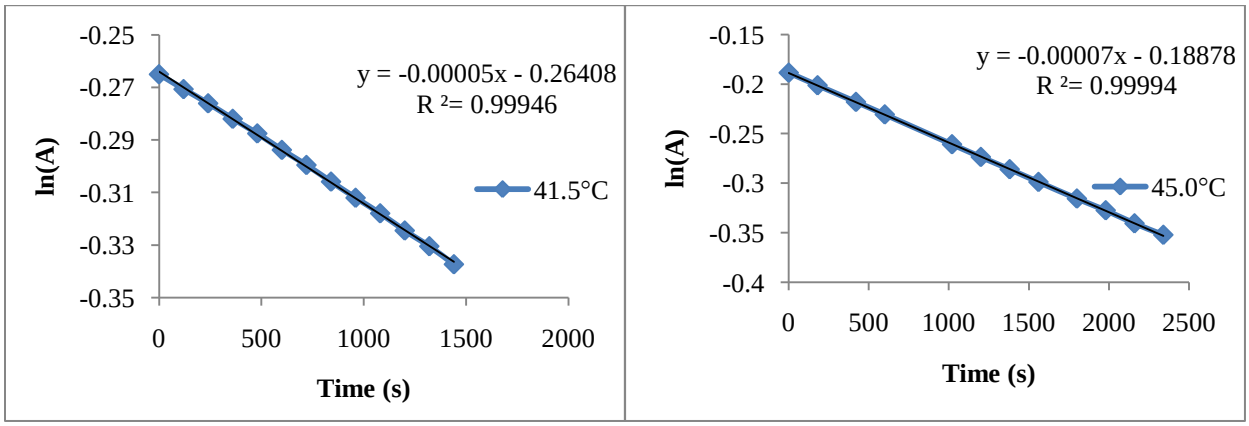

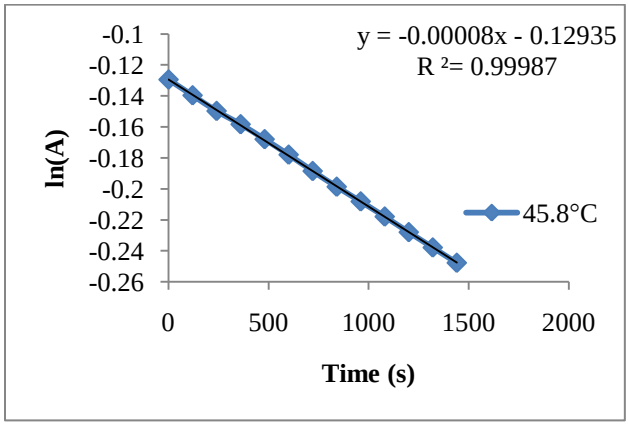

Pyridone 1c

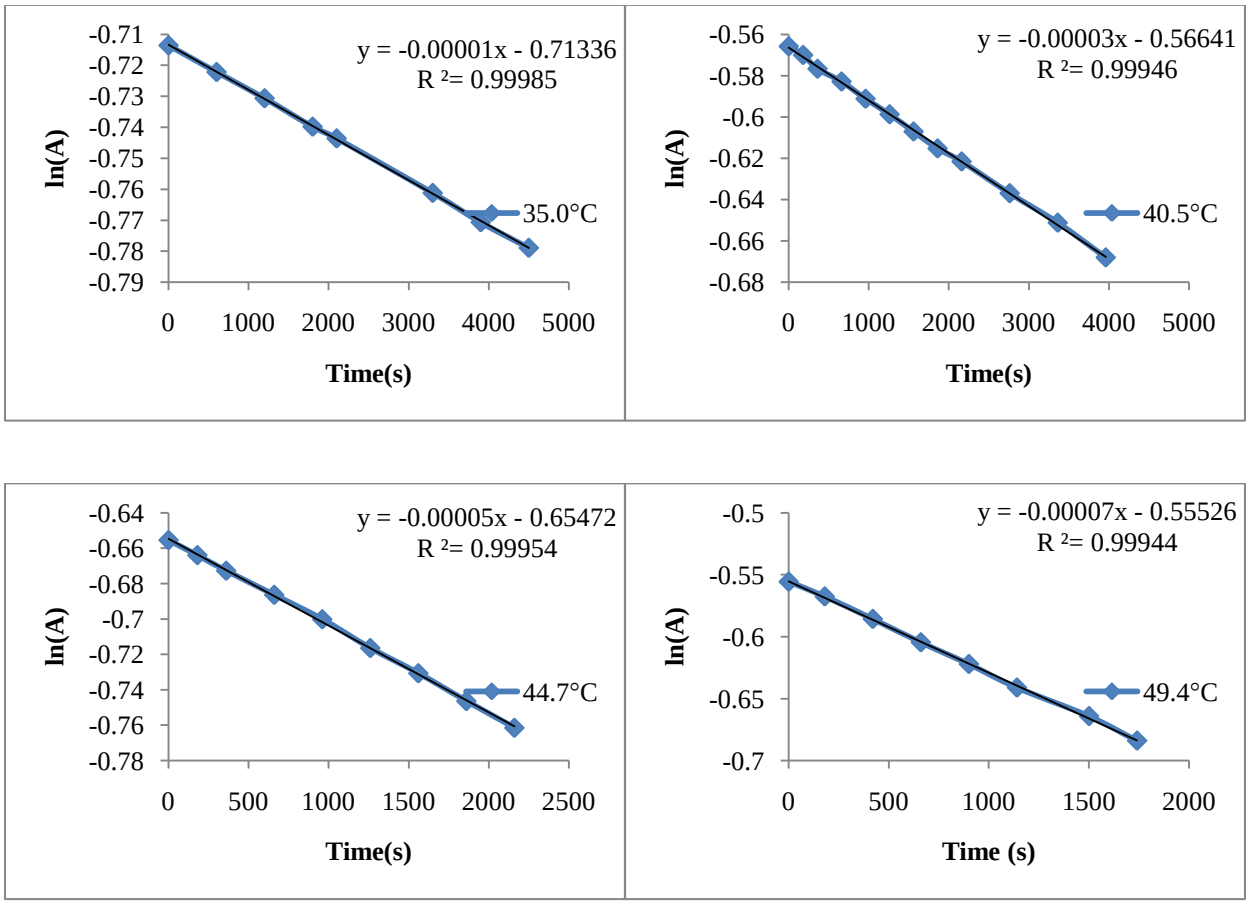
y = -0.00001x - 0.71336
R ²= 0.99985
35.0°C
ln(A)
Time(s)
y = -0.00003x - 0.56641
R ²= 0.99946
40.5°C
ln(A)
Time(s)
y = -0.00005x - 0.65472
R ²= 0.99954
44.7°C
ln(A)
Time(s)
y = -0.00007x - 0.55526
R ²= 0.99944
49.4°C
ln(A)
Time (s)

Pyridone 1d

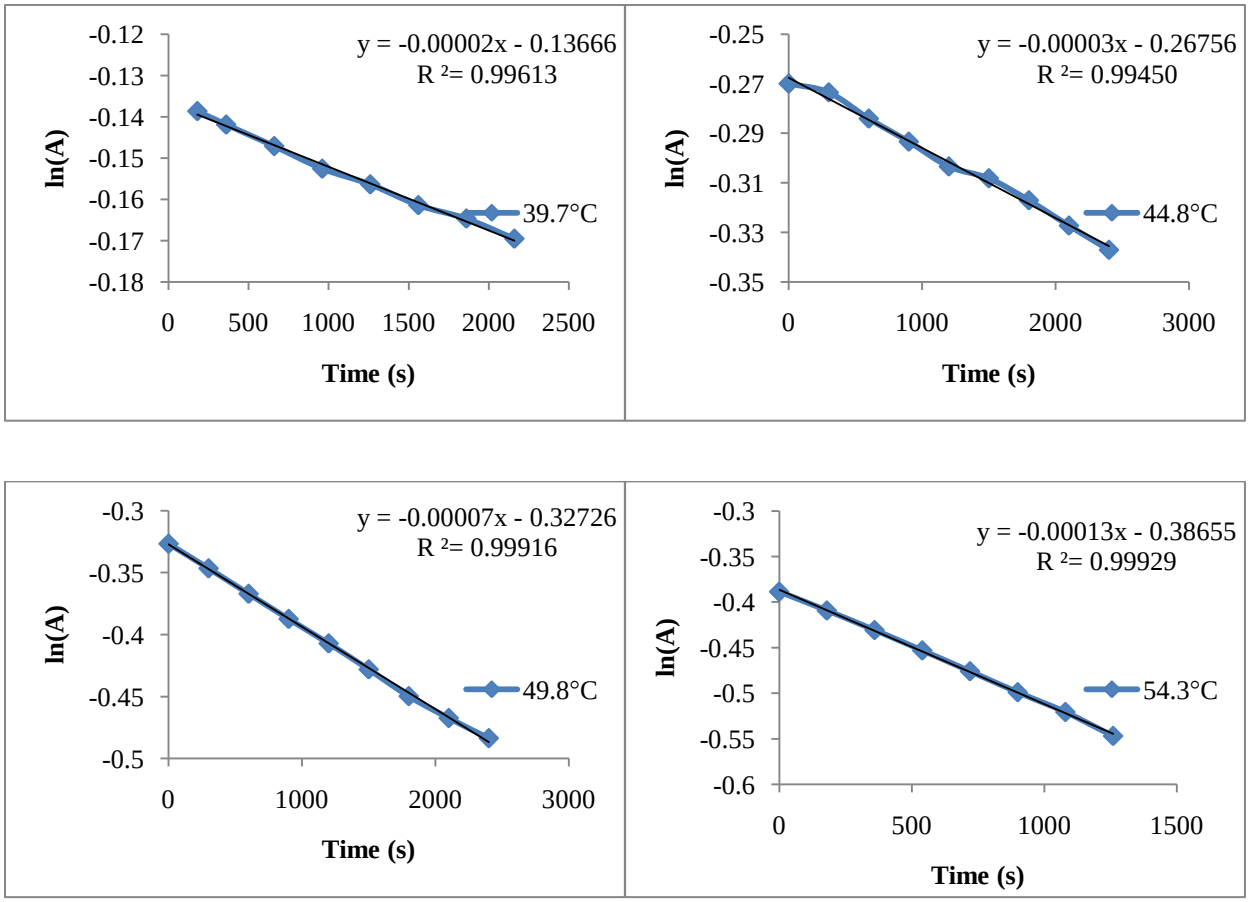
y = -0.00002x - 0.13666
R ²= 0.99613
39.7°C
ln(A)
Time (s)
y = -0.00003x - 0.26756
R ²= 0.99450
44.8°C
ln(A)
Time (s)
y = -0.00007x - 0.32726
R ²= 0.99916
49.8°C
ln(A)
Time (s)
y = -0.00013x - 0.38655
R ²= 0.99929
54.3°C
ln(A)
Time (s)

Pyridone 1e

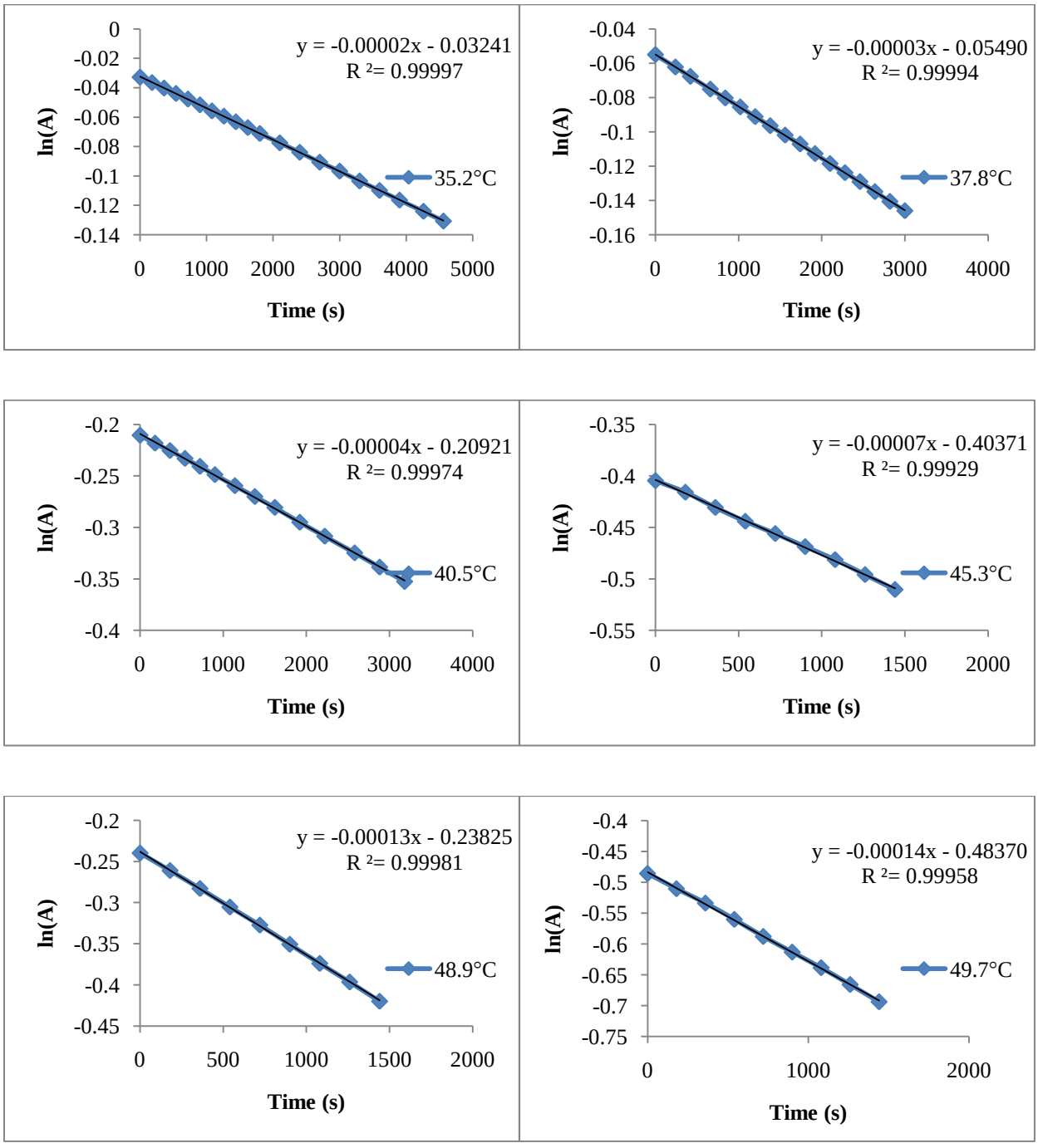
y = -0.00002x - 0.03241
R ²= 0.99997
35.2°C
ln(A)
Time (s)
y = -0.00003x - 0.05490
R ²= 0.99994
37.8°C
ln(A)
Time (s)
y = -0.00004x - 0.20921
R ²= 0.99974
40.5°C
ln(A)
Time (s)
y = -0.00007x - 0.40371
R ²= 0.99929
45.3°C
ln(A)
Time (s)
y = -0.00013x - 0.23825
R ²= 0.99981
48.9°C
ln(A)
Time (s)
y = -0.00014x - 0.48370
R ²= 0.99958
49.7°C
ln(A)
Time (s)

Pyridone 2a

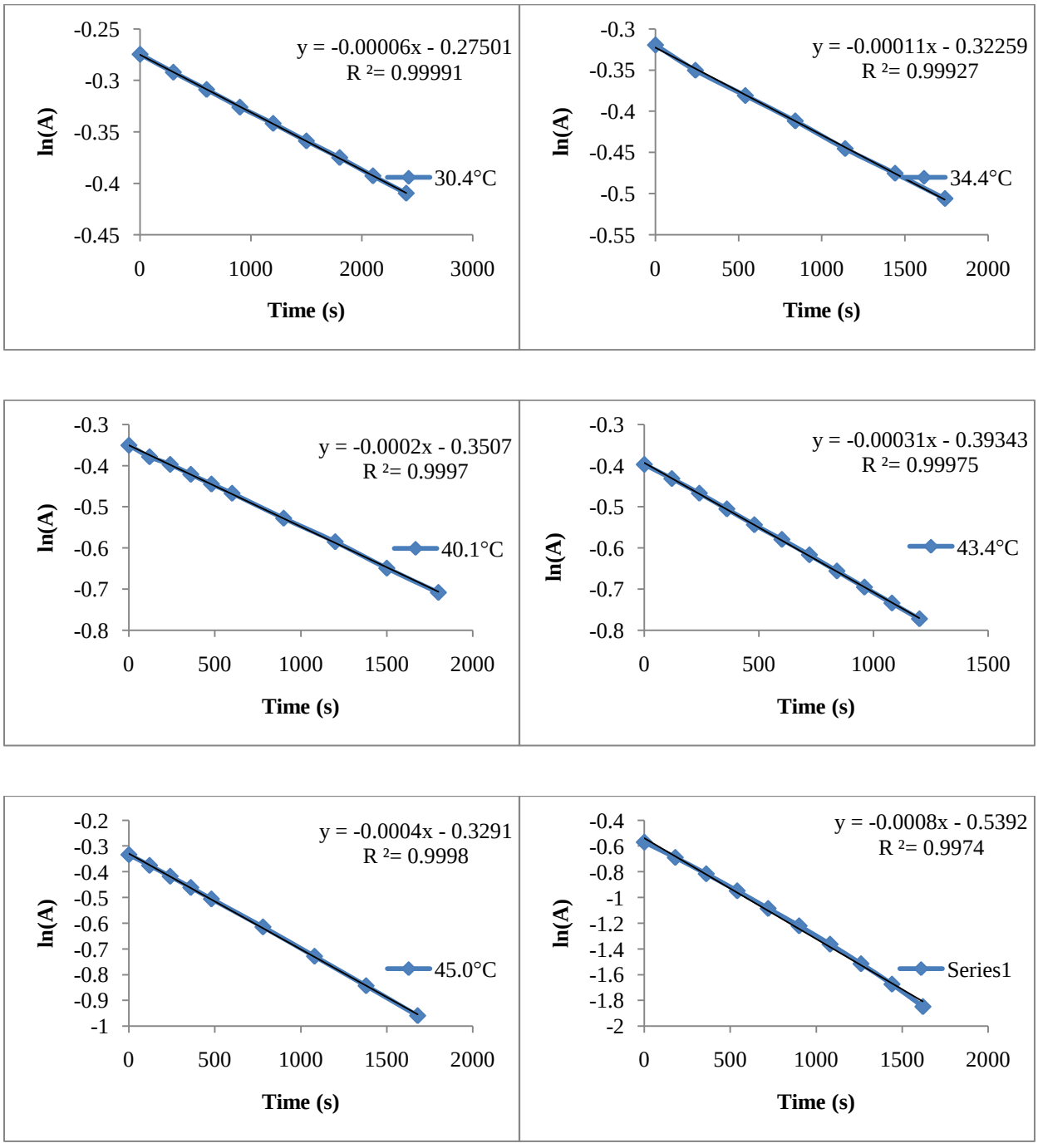
y = -0.00006x - 0.27501
R ²= 0.99991
30.4°C
ln(A)
Time (s)
y = -0.00011x - 0.32259
R ²= 0.99927
34.4°C
ln(A)
Time (s)
y = -0.0002x - 0.3507
R ²= 0.9997
40.1°C
ln(A)
Time (s)
y = -0.00031x - 0.39343
R ²= 0.99975
43.4°C
ln(A)
Time (s)
y = -0.0004x - 0.3291
R ²= 0.9998
45.0°C
ln(A)
Time (s)
y = -0.0008x - 0.5392
R ²= 0.9974
Series1
ln(A)
Time (s)

Pyridone 2d

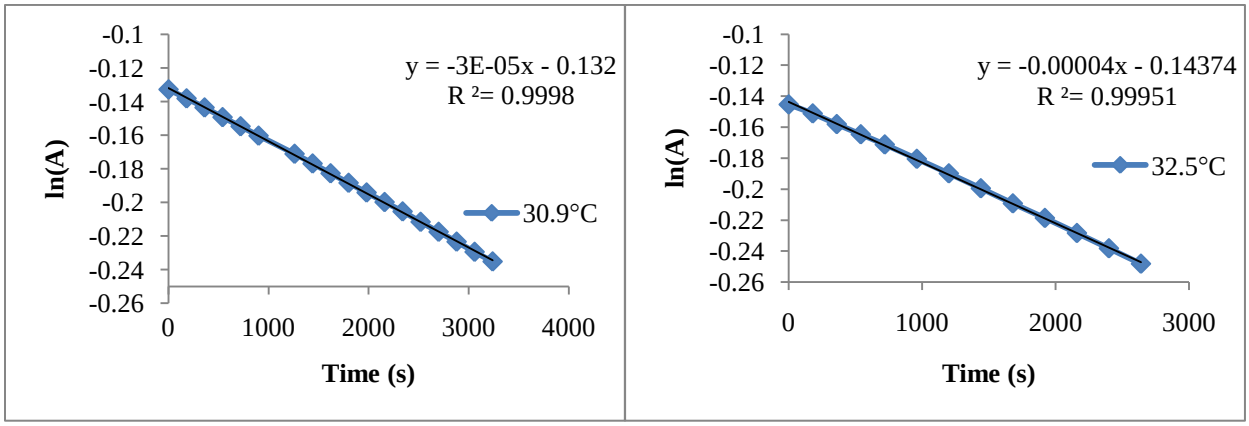
y = -3E-05x - 0.132
R ²= 0.9998
30.9°C
ln(A)
Time (s)
-0.1
-0.12
-0.14
-0.16
-0.18
-0.2
-0.22
-0.24
-0.26
0
1000
2000
3000
4000

y = -0.00004x - 0.14374
R ²= 0.99951
32.5°C
ln(A)
Time (s)
-0.1
-0.12
-0.14
-0.16
-0.18
-0.2
-0.22
-0.24
-0.26
0
1000
2000
3000

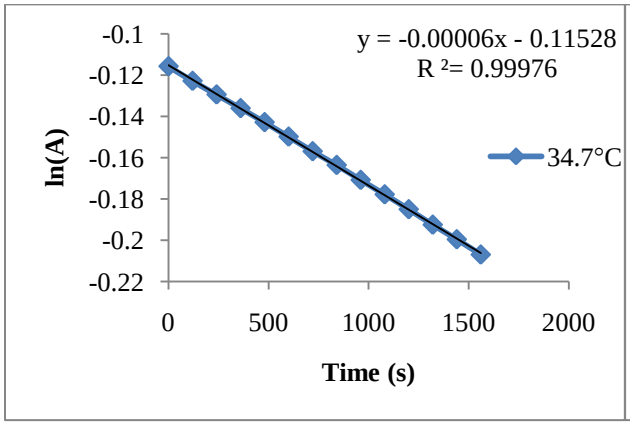
y = -0.00006x - 0.11528
R ²= 0.99976
34.7°C
ln(A)
Time (s)
-0.1
-0.12
-0.14
-0.16
-0.18
-0.2
-0.22
0
500
1000
1500
2000

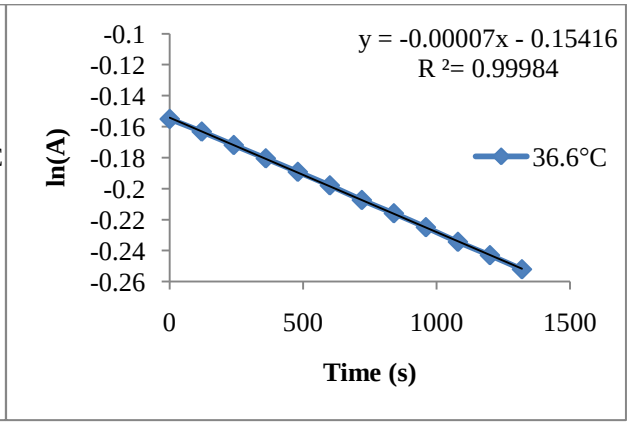
y = -0.00007x - 0.15416
R ²= 0.99984
36.6°C
ln(A)
Time (s)
-0.1
-0.12
-0.14
-0.16
-0.18
-0.2
-0.22
-0.24
-0.26
0
500
1000
1500

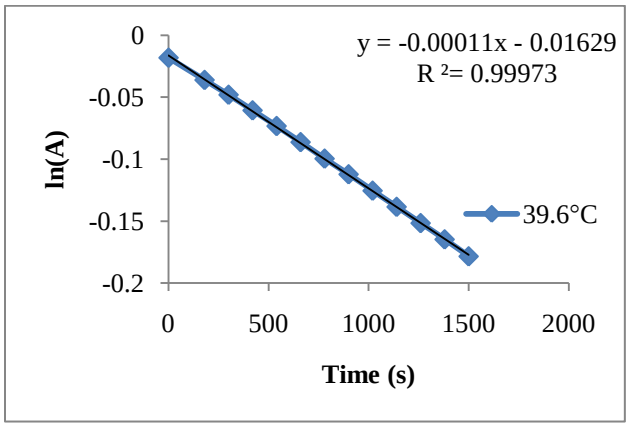
y = -0.00011x - 0.01629
R ²= 0.99973
39.6°C
ln(A)
Time (s)
0
-0.05
-0.1
-0.15
-0.2
0
500
1000
1500
2000

Appendix B – Arrhenius and Eyring Plots

Pyridone 1a

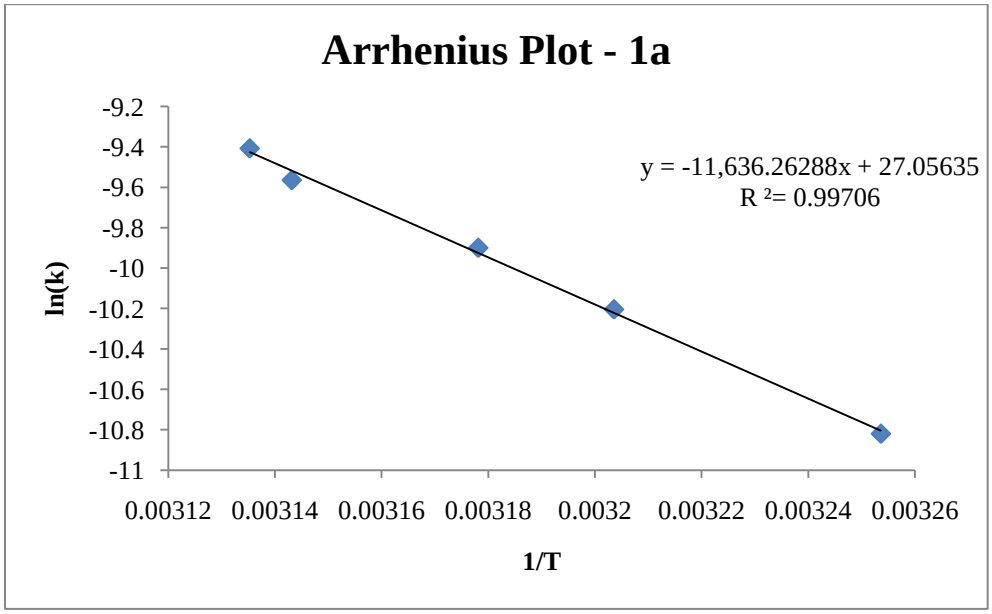

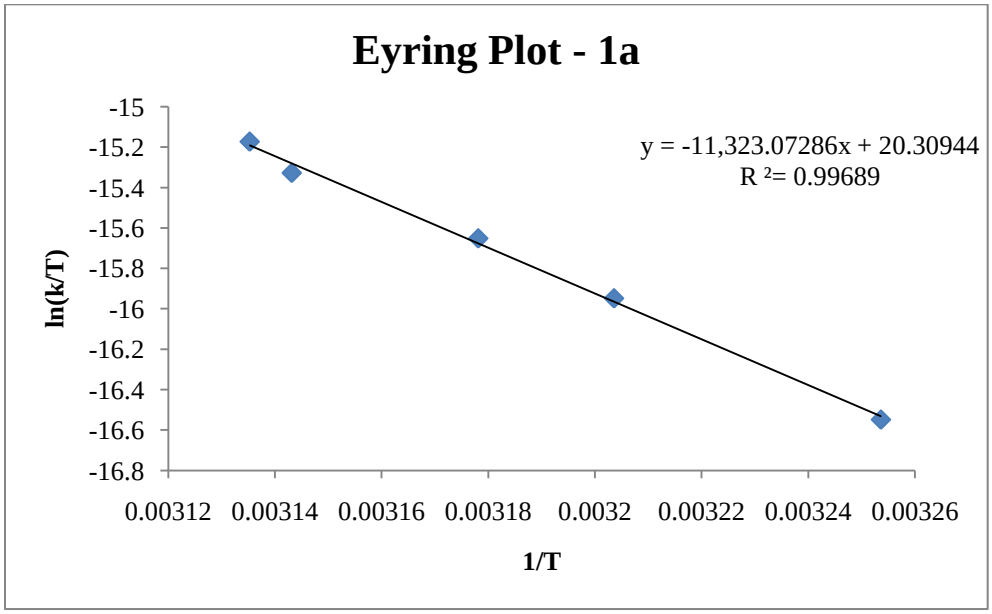

Pyridone 1c

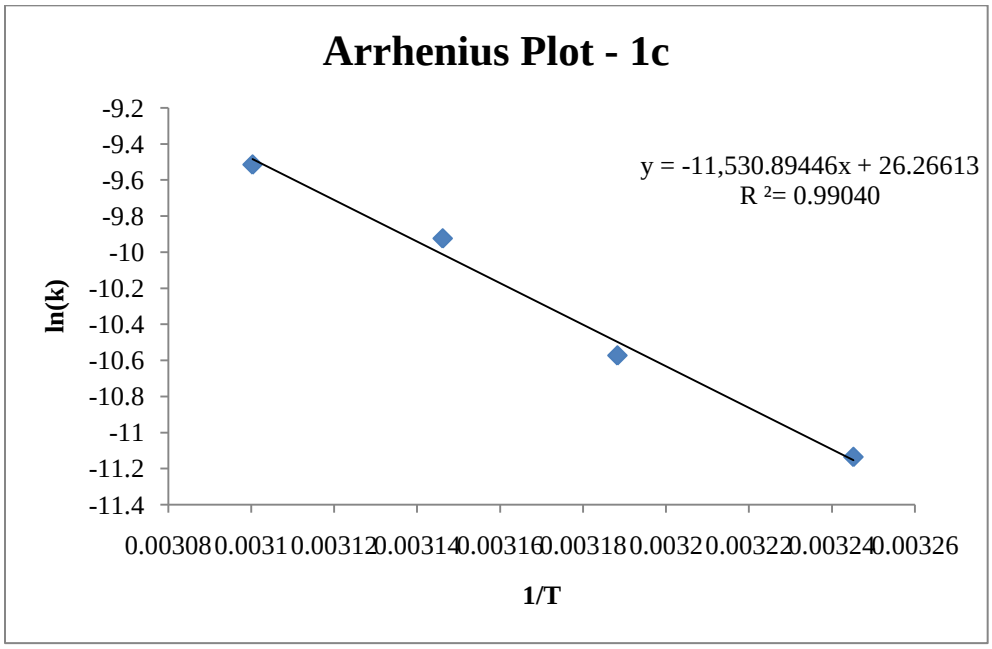
Arrhenius Plot - 1c
y = -11,530.89446x + 26.26613
R ²= 0.99040
ln(k)
-9.2
-9.4
-9.6
-9.8
-10
-10.2
-10.4
-10.6
-10.8
-11
-11.2
-11.4
0.00308 0.0031 0.00312 0.00314 0.00316 0.00318 0.0032 0.00322 0.00324 0.00326
1/T

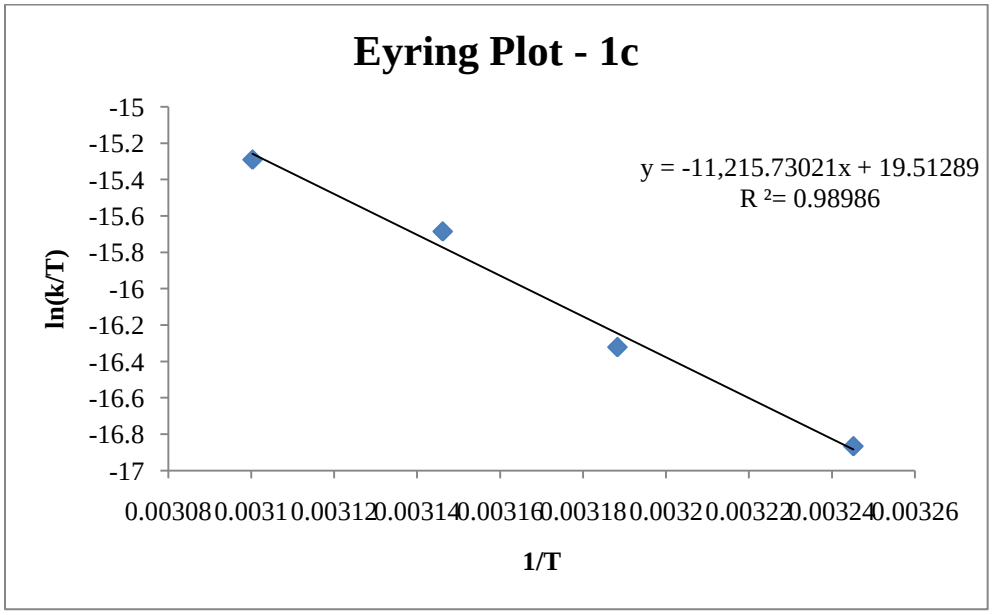
Eyring Plot - 1c
y = -11,215.73021x + 19.51289
R ²= 0.98986
ln(k/T)
-15
-15.2
-15.4
-15.6
-15.8
-16
-16.2
-16.4
-16.6
-16.8
-17
0.00308 0.0031 0.00312 0.00314 0.00316 0.00318 0.0032 0.00322 0.00324 0.00326
1/T

Pyridone 1d

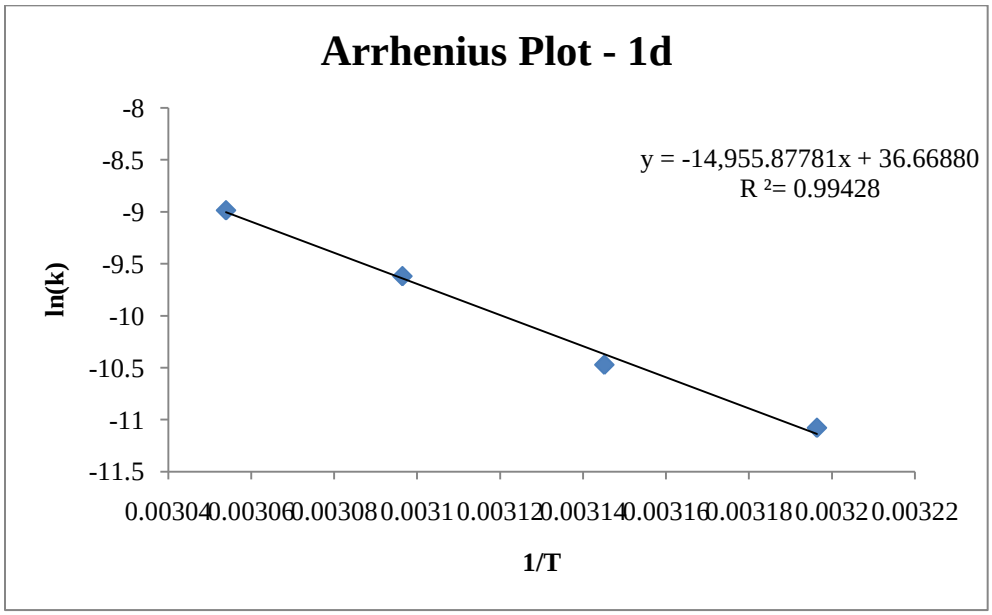
Arrhenius Plot - 1d
y = -14,955.87781x + 36.66880
R ²= 0.99428
ln(k)
-8
-8.5
-9
-9.5
-10
-10.5
-11
-11.5
0.00304 0.00306 0.00308 0.0031 0.00312 0.00314 0.00316 0.00318 0.0032 0.00322
1/T

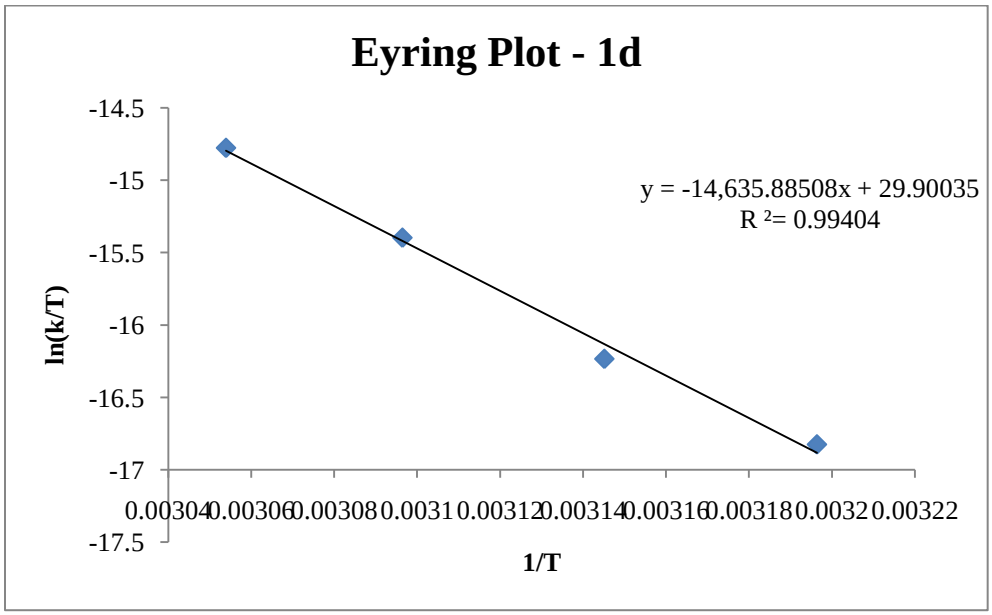
Eyring Plot - 1d
y = -14,635.88508x + 29.90035
R ²= 0.99404
ln(k/T)
-14.5
-15
-15.5
-16
-16.5
-17
-17.5
0.00304 0.00306 0.00308 0.0031 0.00312 0.00314 0.00316 0.00318 0.0032 0.00322
1/T

Pyridone 1e

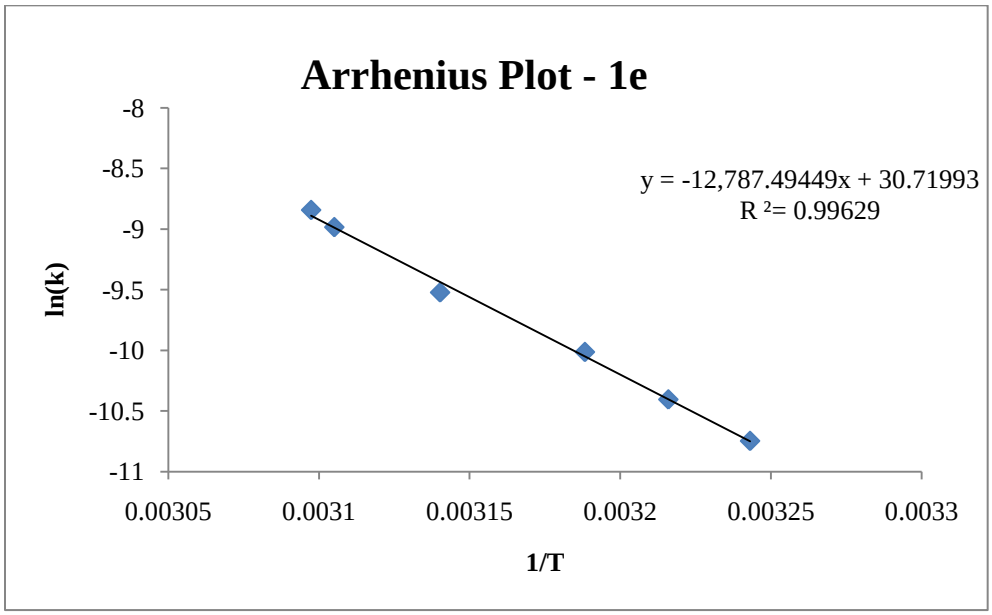
Arrhenius Plot - 1e
y = -12,787.49449x + 30.71993
R ²= 0.99629
ln(k)
-8
-8.5
-9
-9.5
-10
-10.5
-11
0.00305
0.0031
0.00315
0.0032
0.00325
0.0033
1/T

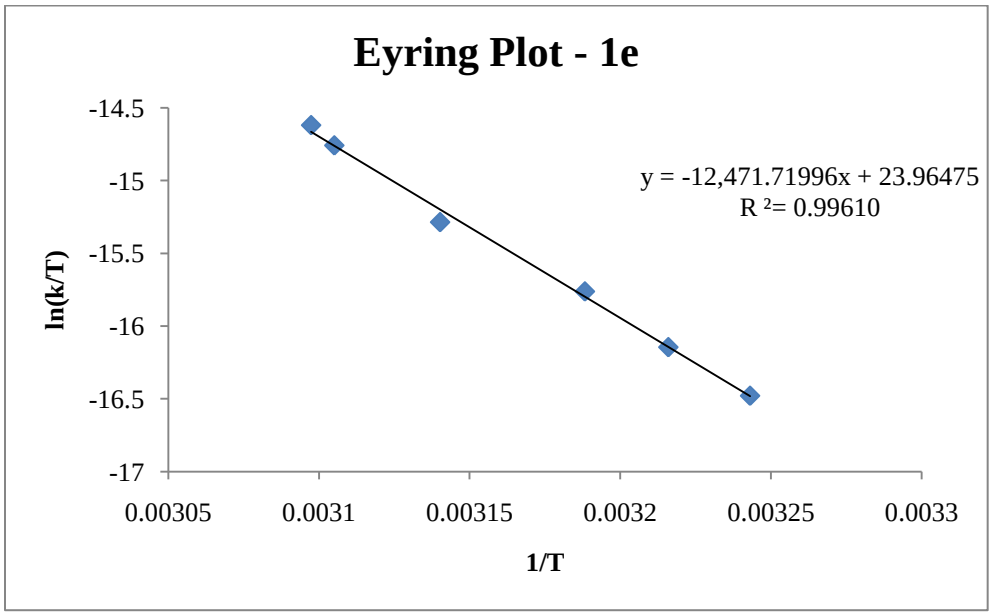
Eyring Plot - 1e
y = -12,471.71996x + 23.96475
R ²= 0.99610
ln(k/T)
-14.5
-15
-15.5
-16
-16.5
-17
0.00305
0.0031
0.00315
0.0032
0.00325
0.0033
1/T

Pyridone 2a

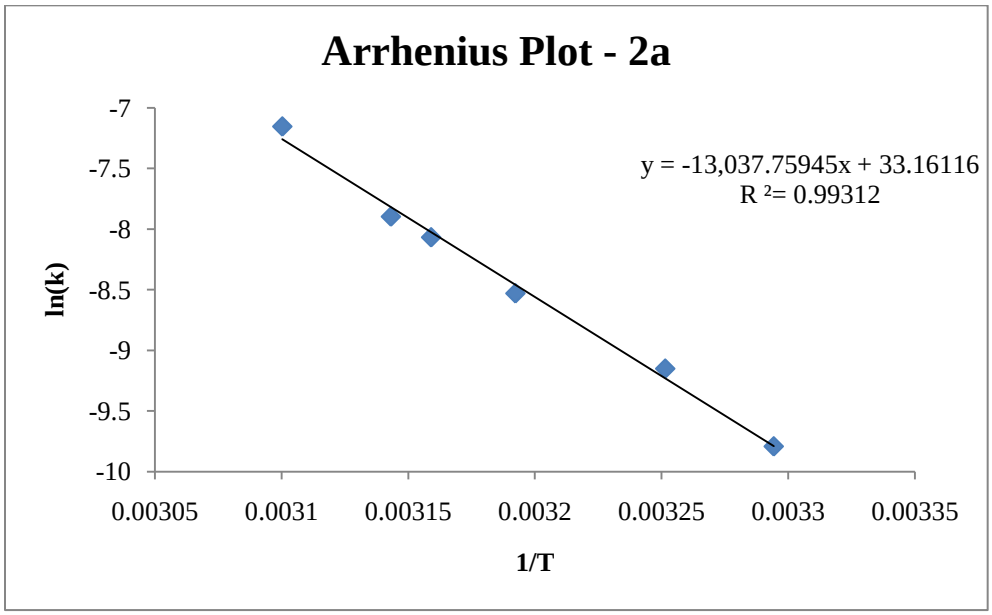
Arrhenius Plot - 2a
y = -13,037.75945x + 33.16116
R ²= 0.99312
ln(k)
-7
-7.5
-8
-8.5
-9
-9.5
-10
0.00305
0.0031
0.00315
0.0032
0.00325
0.0033
0.00335
1/T

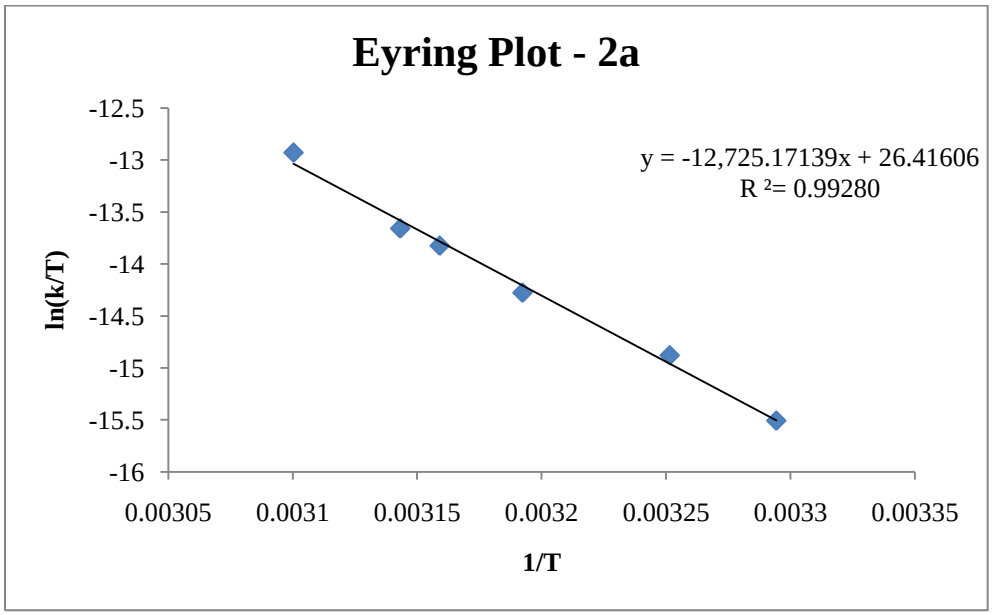
Eyring Plot - 2a
y = -12,725.17139x + 26.41606
R ²= 0.99280
ln(k/T)
-12.5
-13
-13.5
-14
-14.5
-15
-15.5
-16
0.00305
0.0031
0.00315
0.0032
0.00325
0.0033
0.00335
1/T

Pyridone 2d

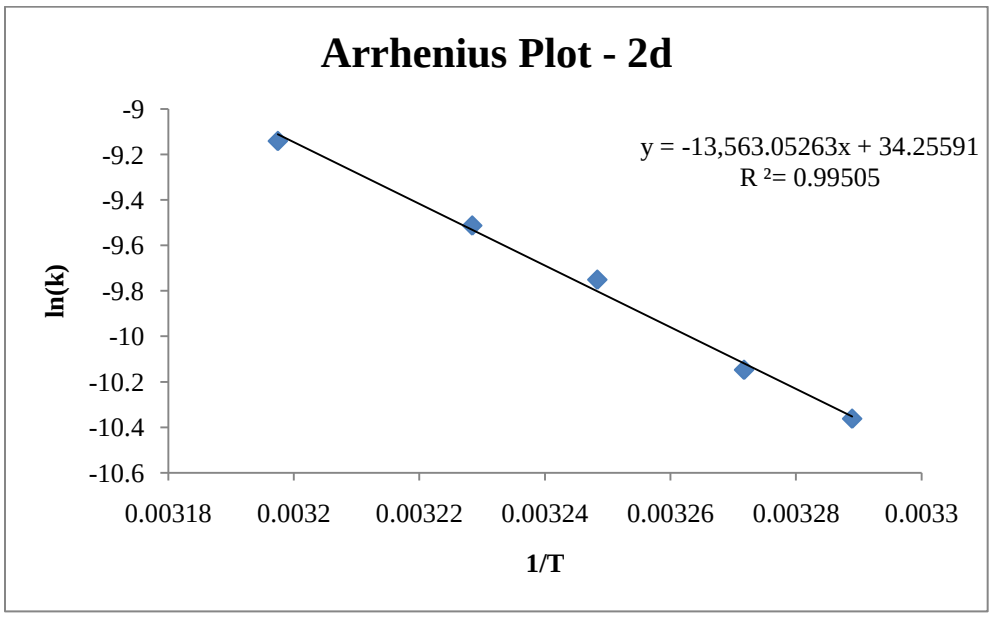
Arrhenius Plot - 2d
y = -13,563.05263x + 34.25591
R ²= 0.99505
ln(k)
-9
-9.2
-9.4
-9.6
-9.8
-10
-10.2
-10.4
-10.6
0.00318
0.0032
0.00322
0.00324
0.00326
0.00328
0.0033
1/T

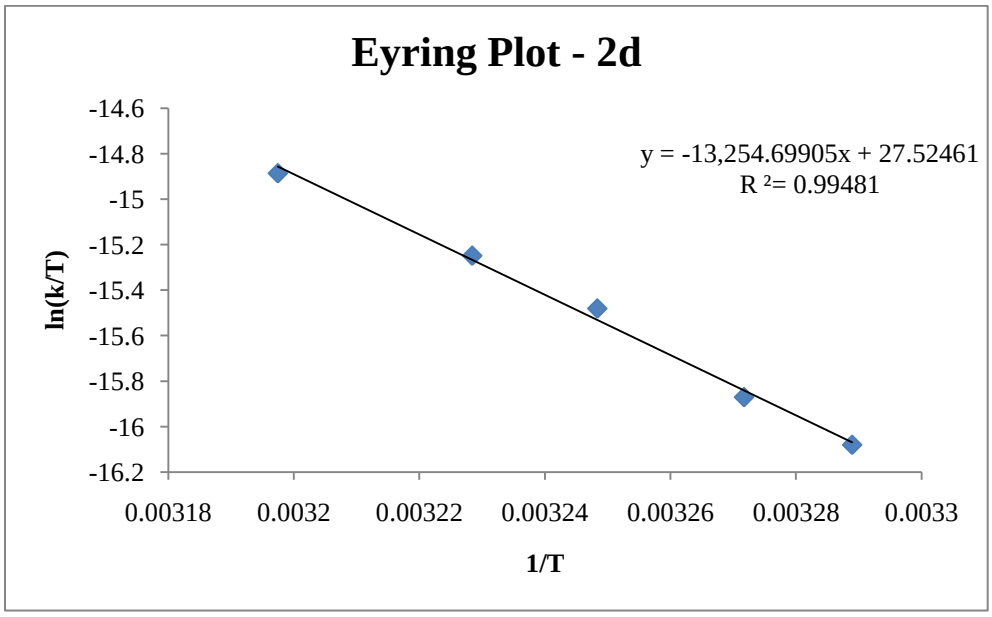
Eyring Plot - 2d
y = -13,254.69905x + 27.52461
R ²= 0.99481
ln(k/T)
-14.6
-14.8
-15
-15.2
-15.4
-15.6
-15.8
-16
-16.2
0.00318
0.0032
0.00322
0.00324
0.00326
0.00328
0.0033
1/T

References

1. Wasserman, H. H.; Wiberg, K. B.; Larsen, D. L.; Parr, J., Photooxidation of Methylnaphthalenes. *The Journal of Organic Chemistry* **2004,** *70* (1), 105-109.
2. Aubry, J.-M.; Pierlot, C.; Rigaudy, J.; Schmidt, R., Reversible Binding of Oxygen to Aromatic Compounds. *Accounts of Chemical Research* **2003,** *36* (9), 668-675.
3. Changtong, C. *Determination of the endoperoxide decomposition rate constant by UV-Vis spectroscopy*; Ventana Research Corporation: Tuscon, AZ, 2009.
4. Harris, D. C., *Quantitative Chemical Analysis*. W.H. Freeman and Company: New York, 1998.
5. Gaussian 09, Revision A.02, M. J. Frisch, G. W. Trucks, H. B. Schlegel, G. E. Scuseria, M. A. Robb, J. R. Cheeseman, G. Scalmani, V. Barone, B. Mennucci, G. A. Petersson, H. Nakatsuji, M. Caricato, X. Li, H. P. Hratchian, A. F. Izmaylov, J. Bloino, G. Zheng, J. L. Sonnenberg, M. Hada, M. Ehara, K. Toyota, R. Fukuda, J. Hasegawa, M. Ishida, T. Nakajima, Y. Honda, O. Kitao, H. Nakai, T. Vreven, J. A. Montgomery, Jr., J. E. Peralta, F. Ogliaro, M. Bearpark, J. J. Heyd, E. Brothers, K. N. Kudin, V. N. Staroverov, R. Kobayashi, J. Normand, K. Raghavachari, A. Rendell, J. C. Burant, S. S. Iyengar, J. Tomasi, M. Cossi, N. Rega, J. M. Millam, M. Klene, J. E. Knox, J. B. Cross, V. Bakken, C. Adamo, J. Jaramillo, R. Gomperts, R. E. Stratmann, O. Yazyev, A. J. Austin, R. Cammi, C. Pomelli, J. W. Ochterski, R. L. Martin, K. Morokuma, V. G. Zakrzewski, G. A. Voth, P. Salvador, J. J. Dannenberg, S. Dapprich, A. D. Daniels, O. Farkas, J. B. Foresman, J. V. Ortiz, J. Cioslowski, and D. J. Fox, Gaussian, Inc., Wallingford CT, 2009.